

A comparison of collocated surface and shallow borehole arrays for microseismic monitoring

Ben Witten¹, Adam Baig¹, Yoones Vaezi²,

¹Nanometrics Inc; ² formerly Nanometrics, now AltaML

Summary

Microseismic monitoring of hydraulic fracture operations with (near-) surface arrays is often hindered by anthropogenic noise sources. Therefore designing optimal monitoring arrays is critical to achieve a successful result. The array choice has been a subject of debate and numerous papers comparing array designs. However, these comparisons are not often one-to-one or are restricted by a limited number of observed events or co-located sensors. Herein we describe a full microseismic data set with a subset of 30 co-located surface arrays and shallow borehole arrays. The data was processed using a larger array and separate streams with only the co-located set of surface arrays and only the shallow borehole arrays over a subset of time. We compare the results through the entire workflow from number of detections through to moment tensor inversions to compare the benefits of each array geometry. The results show that the surface array and shallow borehole array generate similar catalogs. The shallow borehole array has slightly higher signal-to-noise data and less scatter, however this comes at the increased acquisition cost to drill the requisite wells.

Introduction

The choice of monitoring array greatly impacts the quality of results for a microseismic monitoring program. For surface or near-surface arrays, a well-designed array should effectively attenuate the coherent and random noise to improve the signal-to-ratio (SNR) of the data. Thus, an ideal array would have dense spacing of the sensors and complete azimuthal coverage. However, factors such as site accessibility and cost hinder the ability to acquire such arrays. Therefore, compromises are necessary and a suite of potential array designs have emerged. The common array designs are “star”-shaped (Eisner et al. 2011), “patch” (e.g., Schissel -Rebel and Meunier 2013, Roux et al. 2014), “superstation” (e.g. Witten et al., 2019), and shallow borehole arrays (e.g. Smith and Neale 2009). Each array design has its benefits but we will focus on a comparison between a shallow-borehole (SB) array and a superstation array.

While there is no set definition of what constitutes a SB array, this can generally be defined as a set of boreholes with depths of up to approximately 150 m below the surface that each contain one or more geophones (much closer to the surface than the stimulated formations). In terms of microseismic monitoring, the benefit of shallow-borehole arrays is to physically separate the geophone from the noise sources at the surface and locate them below any potentially highly attenuating near-surface layers.

Superstation arrays are comprised of hexagonal arrays of the style described by Witten et al. (2020) with multiple concentric rings of geophone strings. These arrays are designed to attenuate surface waves with a minimal channel count.

Previous studies have examined the differences in array designs between surface and SB arrays, although these comparisons are often limited in the number of co-located arrays and events (e.g. Eisner et al., 2011; Czanik and Eisner, 2013; Witten et al., 2013).

Herein, we present the results from a large set of co-located surface superstation arrays and SB arrays. The co-located arrays are part of a larger monitoring array that recorded the hydraulic fracturing of six wells. This data set serves as a reference for reprocessing of subsets of the stations. The data processing done on the full array was repeated with just the superstation array and the SB array to compare the number of detections, relative locations, magnitudes and moment tensors of the sub arrays to each other and to the reference array.

We begin by describing the data acquired and the processing methodologies. We then detail the results between the SB, superstation, and full reference arrays. While neither the SB array nor the superstation array completely recover the results from the full array due to reduced spatial coverage and channel count, the results are similar. The SB array provides slightly improved results in comparison to the superstation array.

Data Set

A hydraulic-fracture-monitoring project was carried out in the Duvernay formation in NW Alberta Canada over a multi-well pad. The acquisition array consisted of superstations and/or shallow borehole arrays at 81 unique locations. Thirty of the locations had both SB arrays and superstations. Figure 1 shows the array geometry. The red triangles indicate locations with only SB arrays, the blue triangles are only superstations, and the orange diamonds are co-located arrays. We refer to the full acquisition as the reference array. Figure 2a shows the configuration of the SB with 4 geophones at 12, 17, 22, and 27m depths and Figure 2b shows the superstation array configuration. Note that all but 2 superstation arrays had 2 rings (13 geophone strings). The other 2, indicated by the orange diamonds with a black border had 3 rings (19 geophone strings).

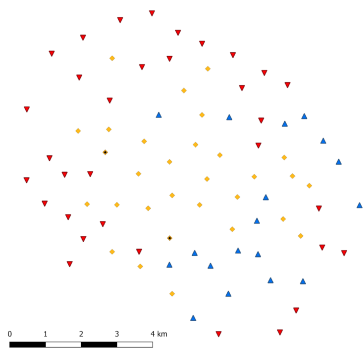


Figure 1: Full array for microseismic monitoring. Red triangles are shallow borehole arrays. Blue triangles are superstation arrays. Yellow diamonds are co-located shallow borehole arrays and superstation arrays.

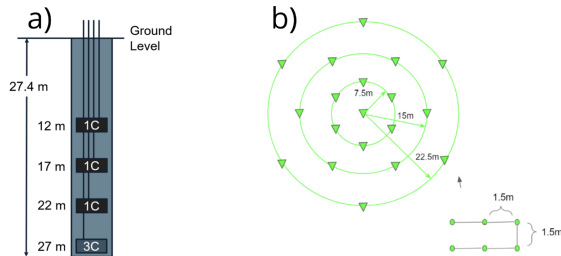


Figure 2: Illustration of individual (a) shallow borehole array and (b) superstation array.

The array recorded for approximately 1.5 months, however only 2 days were chosen to process with the co-located superstation and SB arrays for comparison. During this period 1409 events with magnitudes between $-1.6 < M_w < 0.25$ were detected and located using the full array. The set of 30 superstation arrays and 30 shallow borehole arrays, we will refer to as the surface array and SB array.

Data Processing Methodology

The processing of the reference array and the sub-arrays (surface and SB array) follow the same procedure. The shallow borehole array is further broken down into 4 arrays, where we process the data using only the deepest sensor (SBA1), the deepest two sensors (SBA2), three deepest (SBA3), and sensors at all depths (SBA4).

First the individual traces were despiked and bandpass filtered. For the superstations, a semblance weighted stacking is applied to attenuate coherent noise (Chambers, 2018). We use a modified source-scanning imaging algorithm (Kao and Shan, 2004) to jointly detect and locate microseismic events.

We then apply a time-frequency (TF) denoising algorithm to further attenuate pseudo-stationary noise. Figure 3 shows an example of an event with traces aligned based on moveout before (top) and after (bottom) application of the TF filter. For this event the SNR increases by ~ 7 dB after application of the filter.

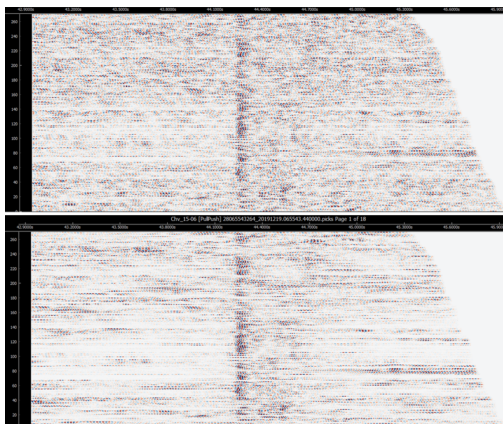


Figure 3: Example event aligned based on event moveout before (top) and after (bottom) time-frequency denoising.

After the filtering, we use template matching to detect smaller events that were not captured during the imaging phase. After both imaging and template matching manual QC is performed to ensure that all detections are from seismic events.

We compute moment magnitudes (M_w) for each event. For larger events, the data is fit assuming a Brune model. Smaller event magnitudes are estimated

through Mw to imaged amplitude fit (Baig et al., 2019). Finally, moment tensors along with confidence parameters are computed for each event as described in Baig et al. (2020).

For the superstation and SB arrays we examine numerous parameters in relation to the reference array, which is assumed to be the most complete and accurate. We compare the number of events, false positive rate, signal-to-noise ratio, event location and uncertainty estimate, moment magnitude, moment tensor results.

Results

Table 1 shows the number of events detected and false positive rate for each sub array. The number of events is the true positive event count after manual QC of the data. Despite the reduction in channel count all sub arrays perform reasonably comparably to the reference array detecting between 85% and 94% of the reference catalog and a false positive rate between 74% and 82%. Interestingly, the addition of the two shallowest geophones does not improve the number of events, with the shallowest reducing the event detections. This result suggests the shallow sensors are noisy and a detriment to the SNR.

| Array | Number of events | % of reference | % false positive |
|-----------|------------------|----------------|------------------|
| Reference | 1409 | | |
| Surface | 1192 | 85 | 82 |
| SBA1 | 1280 | 91 | 76 |
| SBA2 | 1326 | 94 | 80 |
| SBA3 | 1326 | 94 | 81 |
| SBA4 | 1304 | 93 | 74 |

Table 1: Comparison of number of events and false positive rate for sub arrays.

Figure 4 shows a histogram of detected events in magnitude bins from the reference array along with missed events for each sub array. All arrays detected the larger magnitude events, as expected, but failed to detect some of the smaller events due to reduced channel count compared to the reference array.

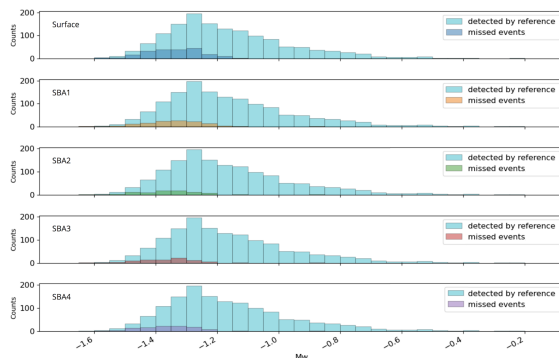


Figure 4: Histogram of detected and missed event reference magnitude for each sub array.

deepest borehole geophone. After the TF

filter the borehole geophone SNR increases more

than the surface array indicating more predictable noise at depth. Once all noise removal steps are applied the lowest two borehole geophones have higher SNR than the surface array.

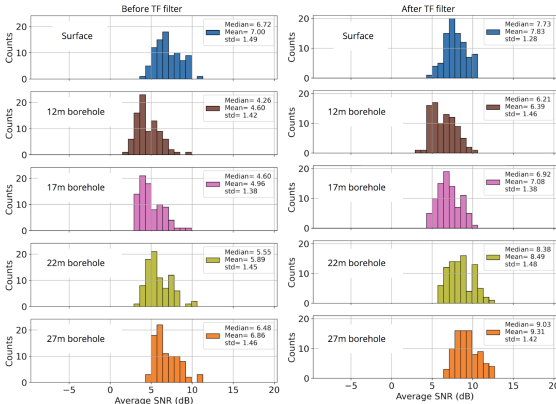


Figure 5: Histogram of average SNR for events detected on (from top to bottom) the surface array, then shallow to deepest borehole geophone before (left) and after (right) TF filtering.

Table 2 shows the median absolute difference in locations for the superstation and SBA1 arrays from the reference array in addition to the median horizontal and vertical uncertainty values. Both the surface and SBA1 arrays have larger uncertainty values than the reference array. This is due to the smaller channel count and limited aperture of these arrays compared to the reference. The location errors between the sub arrays are within 10m of each other in both the horizontal and vertical directions. The SBA1 array has a smaller difference likely due to the higher SNR observed on this array. Larger events on both arrays had smaller and similar location differences as well as uncertainty values.

| Array | Median XY difference from reference (m) | Median Z difference from reference (m) | Median XY uncertainty (m) | Median Z uncertainty (m) |
|-----------|---|--|---------------------------|--------------------------|
| Reference | | | 20.8 | 34.5 |
| Surface | 83.1 | 102.0 | 40.1 | 65.3 |
| SBA1 | 70.6 | 91.0 | 40.3 | 64.4 |

Table 2: Comparison location and location uncertainty for surface and SBA1 sub arrays relative to the reference array.

For the calculation of moment tensors and moment magnitudes, we apply a different denoising procedure. To ensure correct and consistent amplitudes, we use a simple stack rather than the semblance weighted stack to collapse the superstations and the TF filter is not applied to any of the arrays.

To calculate the moment magnitudes, we fit the largest events to the Brune model and then estimate the magnitude of smaller events by deriving a relationship between magnitude and imaged amplitude. For the events fit to the Brune model, we observe a consistent over estimation of the magnitudes by approximately 0.1 Mw units across all shallow borehole array groups (SBA1, SBA2, etc.) in comparison to the reference array. While the surface array

matches much more closely to the reference array, with a median difference of only 0.01 Mw units.

As noted above, the method we use for moment tensor inversion outputs not just the solution and R-value, but also a confidence value that controls for differences in number of sensors. Table 3 shows the number of events with resolved moment tensors greater than 95% confidence. The surface array outperforms SBA1 and SBA2 but is worse than SBA3.

By adding more stations to the borehole arrays, the number of events that is confidently resolved increases until the shallowest geophone is added. This result is consistent with the event count. For both arrays, the resulting ensemble of monitor tensor solutions provides similar interpretive value and results.

| Array | # of events |
|---------|-------------|
| Surface | 203 |
| SBA1 | 131 |
| SBA2 | 198 |
| SBA3 | 238 |
| SBA4 | 170 |

Table 3: Number of events with moment tensor solutions greater than 95% confidence for each sub array.

As mentioned previously, two of the superstations (denoted with the black outline in Figure 1) had 19 geophone strings (3 rings). From these locations, a comparison was done to reduce the channel count to 2 and 1 ring, 13 and 7 geophone strings, respectively. The 19 node superstation had higher SNR than all but the deepest borehole geophone, while the 13 and 7 node arrays outperform the two shallowest borehole geophones.

Acknowledgements

We are grateful to the anonymous owners of the data for permission to publish these results. We also thank our colleagues for helping prepare this analysis.

References

- Baig A., B. Witten, S. Karimi, D. Baturan, and E. Yenier, (2019), Magnitude calibration of imaging-based microseismic locations, SEG Technical Program Expanded Abstracts: 3086-3090.
- Baig A., B. Witten, S. Karimi, (2020), Quality Control of Microseismic Moment Tensors from Surface-Based Acquisitions, GeoConvention Expanded Abstracts: 1-6.
- Chambers, K.,(2018), Noise attenuation in sparse-surface microseismic datasets, SEG Technical Program Expanded Abstracts: 2902-2906.
- Czanik, C. and L. Eisner, (2013), Signal and Noise on Buried and Surface Geophones for Microseismic Monitoring, 75th EAGE Conference & Exhibition, 348-00939.
- Eisner, L., S. Williams-Stroud, A. Hill, P. Duncan, and M. Thornton, (2010), Beyond the dots in the box: Microseismicity-constrained fracture models for reservoir simulation: The Leading Edge, 29, 326–333.
- Eisner, L., A. De La Pena, S. Wessels, W. Barker and W. Heigl. (2011), Why Surface Monitoring of Microseismic Events Works, Third EAGE Passive Seismic Workshop - Actively Passive, 225-00008.

- Kao, H. and S. Shan, (2004), The Source-Scanning Algorithm: mapping the distribution of seismic sources in time and space, *Geophysical Journal International*, 157:2, 589–594
- Roux, P.-F. and Kostadinovic, J. and Bardainne, T. and Rebel, E. and Chmiel, M. and Van Parys, M. and Macault, R. and Pignot, L., (2014), Increasing the accuracy of microseismic monitoring using surface patch arrays and a novel processing approach, *First Break*, 32:7.
- Schissel -Rebel, E. and J. Meunier, (2013), Patch versus broadband networks for microseismic: A signal-to-noise ratio analysis, *SEG Technical Program Expanded Abstracts* : 2104-2108.
- Smith, P., C. Neale, (2009), The use of large aperture buried geophone arrays for high efficiency stimulation and production microseismic monitoring, *AAPG Annual Convention and Exhibition*.
- Witten, B., R. M. Habiger, and B. Artman, (2013), A technical and economic value analysis of shallow borehole arrays for microseismic monitoring, *SEG Technical Program Expanded Abstracts* : 2109-2113.
- Witten, B., A. Booterbaugh and R. Segstro, (2019), A Novel Array Acquisition and Processing Methodology for Microseismic Monitoring, *81st EAGE Conference and Exhibition*: 1 - 5.
- Witten, B., A. Baig, S. Karimi, and G. Purdue, (2020), "Surface microseismic acquisition and processing with a lightweight array," *SEG Technical Program Expanded Abstracts* : 2049-2053.